Journal of Information Engineering and Applications
ISSN 2224-5782 (print) ISSN 2225-0506 (online)
Vol.3, No.9, 2013

3-Dimensional Nonlinear Finite Element Analysis of both Thermal and Mechanical Response of Friction Stir Welded 2024-T3 Aluminum Plates

Dr.Kareem N. Salloomi, Dr. Laith Abed Sabri, Yahya M. Hamad, Sanaa Numan Mohammed
University of Baghdad, Al-Khwarizmi College of Eng, Automated Manufacturing Eng
kareemsalloomi@yahoo.com, laith_phd@yahoo.com, yahya_m_hamad@yahoo.com.au,
sanaaalsumaidae@yahoo.com

Abstract
This paper attempt to predict numerically both the temperature distribution during friction stir welding process of 2024-T3 aluminium plates and the resulting thermal residual stress by sequentially coupling the thermal histories into the mechanical model assuming elastic-perfectly plastic metal behaviour in accordance with the classical metal plasticity theory. The commercial code ANSYS 14 is used in Thermomechanical modelling of friction stir welding of aluminium 2024-T3. Heat input from the tool shoulder and the tool pin are considered in the finite element analysis model. A moving heat source with a heat distribution simulating the heat generated from the friction between the tool shoulder and the work piece is used in the heat transfer analysis The longitudinal stress components are found to be the highest tensile stress components and correspond to the temperature profiles within the heat affected zone of the weld. The through-thickness (normal) stresses are found to be negligible compared with the longitudinal and transverse stress components. To facilitate simulation runs of the proposed model an APDL (ANSYS Parametric Design Language) code is developed to extract the thermal history and the subsequent thermal stresses. The effects of various heat transfer conditions at the bottom surface of the workpiece, thermal contact conductances at the work-piece and the backing plate interface on the thermal profile in the weld material are taken into considerations. The results of the simulation are compared to other published experimental results and the agreement was good.
Keywords: Friction stir welding, Finite element, Three dimensional modeling, Thermal stresses.

1. Introduction

FSW was the parent technology invented by Thomas et al. in 1991.FSW is a solid state welding process performed at temperatures lower than the melting point of the alloy. The workpieces are rigidly clamped in a fixed position and a specially profiled rotating tool traversed through the joint line produces the friction heating. The tool is crushing the joint line, breaking up the oxide film by a mechanical stirring and forging of the hot and plastic material. The resulting joint exhibits a finer grain structure than the base metal. This technology has taken off in a number of applications due to a number of benefits, Apart from these advantages, it can be considered as enabling technology for joining of high strength aluminum alloys which are classified as unweldable by fusion welding techniques. Other advantages are welding include the absence of issues relating to the cooling phase, such as solidification cracking. Friction stir welding also offers better safety due to lack of toxic fumes and produces a lower environmental impact. Applications of FSW can be found in the shipbuilding, aerospace and automotive industries. A schematic representation of the FSW process is shown in Fig. 1.
FSW is based on strong couplings of thermo-mechanical phenomena. It induces very complex material motions and large shear forces. The material temperature is raised to about 80% of the melting temperature [1,2]. Being a recent and under- development process, Its numerical simulation is expected to aid a better understanding of its physics, observing the influence of the input parameters on the obtained joints, and optimizing the overall process for a large range of tools, process conditions and materials. However, the development of a satisfactory numerical model requires deep efforts and much time. So far, only limited information has been available about the residual stress distribution in friction stir welds. Most of the investigations have been experimentally based [3-5].Sutton [6] investigated the residual stress in 2024-T3 aluminum friction stir butt welds using the neutron diffraction technique, and the results indicated that the highest stresses occur near the crown side of the weld over the entire FSW joint region. Rui M. Leal and Altino Loureiro [7] studied the effect of the welding process on the microstructure and mechanical properties of friction stir welded joints in aluminum alloys 2024- T3, 5083-O and 6063-T6, a small loss of hardness and strength was obtained in welds in alloys 2024-T3. Webster and et al. [8] reported the measurement of residual stress in FSW by X-ray technique, which shows that the longitudinal residual stress varies in the range from 60 to 140MPa, and also shows a correlation between the detailed residual stress feature and the heat flow in the weld. Many variations in the process of FSW make it difficult to conduct a thrill investigation. Major, independent variables are: rotational speed of the tool, tool advancing speed, magnitude of downward force to hold the touch between tool and piece steady, tool geometry, and tilt angle and type of material (thermo physical properties). These variables affect heat distribution as well as

residual stress and mechanical properties of the connection. A portion of the generated heat disseminated through work piece, will affect distortion, residual stress distribution as well as weld quality of the piece. Chao and etal [9] investigated the variations of heat energy and temperature generated by the FSW, the study showed that only about 5% of the heat generated by the friction process flows to the tool and the rest flows to the work piece. Jweeg and etal [10] investigated theoretically and experimentally transient temperature distribution in friction stir welding of AA 7020-T53.

In this study, we present an integrated nonlinear thermal-mechanical model to analyze both temperature and residual stress distributions in friction stir welds of heat-treatable aluminum alloy Al2024-T3. This integrated approach can be used to quantify the effects of welding process conditions on the residual stress and microhardness distributions in the friction stir weld.

2. Non-Linear Finite Element Modeling of FSW

2.1 Thermal Analysis

A three dimensional transient, isotopic solid with moving heat source finite element model was developed to simulate the friction stir welding process in Al 2024-T3 using the commercial code ANSYS13. As a first step in the analysis the transient temperaturefield T which is a function of time t and the spatial coordinates (x,y,z),is solved[11]

$$\left\{k(T)\left(\frac{\partial^2 T}{\partial x^2}\right)+\left(\frac{\partial^2 T}{\partial y^2}\right)+\left(\frac{\partial^2 T}{\partial z^2}\right)\right\}+\dot{Q}=\rho(T)C_p(T)\left(\frac{\partial T}{\partial t}\right) \qquad (1)$$

where,

ρ Density, kg/m^3 ,C specific heat J/kg°K

K Thermal conductivity along x, y, and z directions, W/m°K

T Absolute temperature, K

$\dot{Q}$ is rate of heat generation

Modeling heat evolution between the tool and welded plate is an important step in understanding how it affects material flow and microstructure modification within and surrounding the weld. To compensate for the lack of a predicted temperature field, measured temperature values from an actual FSW test [15] are used to construct an approximate temperature field for the FSW process. This temperature field is then used as input for the solid mechanics model for the same FSW process. As such, a problem geometry that accommodates the simulation of the preceding FSW test is used.. The whole FSW process including plunge, dwell, traverse, pull out and cooling stages are modeled.

During the process the tool travels at a constant speed ($V_{t)}$ this motion is simulated by changing heat source location as shown in figure 2 according to the following equation

$X_{i+1} = X_i + V_t \Delta t$ ……..(2)

Where Δt is the time required for the tool to travel from location $X_i$to X_{i+1}, (i.e element size) and V_t is the tool traveling speed.

2.2.1Geometry

Two sheets are modeled with each sheet having dimensions of 0.305m*0.105m*0.008m. Figure 3 shows the modeled geometry.

2.2.2Model Mesh

SOLID70 which is a three-dimensional thermal solid, is used as the element type for analysis. SOLID70 has a three dimensional thermal conduction capability. The element has eight nodes with a single degree of freedom, temperature, at each node. The element is applicable to a three dimensional, steady-state, or transient thermal analysis. The element also can compensate for mass transport heat flow from a constant velocity field. If the model containing the conducting solid element is also to be analyzed structurally, the element should be replaced by an equivalent structural element such as SOLID45. For the consideration of the radiation effect on the plate surface, a three dimensional thermal surface effect element (SURF152) is used overlaying it onto the faces of the base elements made by SOLID70. Figure 3b shows the geometry, node locations, and the coordinate system of the element, which is defined by four to nine nodes and the material properties (e.g., emissivity). An extra node has to be created to investigate the radiation effect, which is positioned away from the base element. For mechanical analysis, a structural element defined by eight nodes (i.e., SOLID45) is used for three dimensional modeling of the plate. Each node of the element has three degrees of freedom: translations in the nodal x, y, and z directions. The element supports analysis of plasticity, large deflection, large strain, stress stiffening, creep and swelling. For the structural analysis, the heat transfer model containing the equivalent thermal element SOLID70 can be replaced by this element, and temperatures obtained from the thermal step can be applied as element body loads at the nodes. The geometry, node locations, and the coordinate system of this element are equal to the SOLID70 (See Figure 4 a). Figure (5) shows the meshes generated for the present simulation. The meshes are

composed of a total number of 80,000 solid elements and 20,000 surface elements.

2.2.3 Material Properties

Thermal conductivity, K and heat capacity, C are dependent on temperature. The ambient temperature was assumed to be 25°C. The initial temperature of the workpiece is assumed to be equal to the ambient temperature. As can be seen in Eq.(1), temperature response in a material involved in high heat fluxes is determined by the thermal material properties of thermal conductivity, specific heat, and density, which are dependent on temperatures. The accurate calculation of temperatures is critical in friction stir welding because bending variables of stress and strain are dependent on temperatures. Therefore, temperature dependent thermal and mechanical properties of Al-2024-T3 plate are used in the finite element model. The thermal and mechanical material properties of Al 2024-T3 are presented in table [1], after Ref. [13]

2.2.4Boundary Conditions

The boundary and initial conditions that are applied to the heat transfer model shown in Fig. 6 are given as follows

The boundary conditions used include:

- Adiabatic condition is considered on the laser path due to symmetry.
- Heat losses from the plate surfaces to the surroundings take place by means of natural convection and radiation effects.

For the radiant heat loss, q_r,

$$q_r = \sigma\varepsilon_r(T_r^4 - T_\infty^4) \text{……..(3)}$$

Where:

σ= the Stefan-Boltzmann constant (σ=5.67*10^{-8} $W/m^2.K^O$)

ε_r = the emissivity of radiating surface (ε_r=0.5)

Tr = the absolute temperature of radiating surface

T_∞ = the absolute temperature of surrounding (T_∞=298 K^O)

For the convective heat loss, q_c,

$$q_c = h_f(T_S - T_\infty) \text{……..(4)}$$

Where:

h_f = the convection coefficient (h=30 $W/m^2.K^O$)

Ts = the temperature at the plate surfaces

2.2.5 Mechanical Analysis

In the thermo-mechanical analysis, the incremental theory of plasticity is used. The plastic deformation of the materials is assumed to obey the von Mises yield criterion and the associated flow rule. The relationship of the rate components between thermal stresses, σ_{ij} , and strains, ε_{ij} , is described by

$$\dot{\varepsilon}_{ij} = \frac{1+\nu}{E}\dot{\sigma}_{ij} - \frac{\upsilon}{E}\dot{\sigma}_{kk}\delta_{ij} + \lambda s_{ij} + \left[\alpha + \frac{\partial\alpha}{\partial T}(T - T_0)\right]\dot{T} \text{……(5)}$$

where E is the Young's modulus, ν is the Poisson's ratio, α is the thermal expansion coefficient, $s_{ij} = \sigma_{ij} - 1/3\sigma_{kk}\delta_{ij}$ are the components of deviatoric stresses and λ is the plastic flow factor. $\lambda = 0$ for elastic deformation or $\sigma_e < \sigma_s$, and $\lambda > 0$ for plastic deformation or $\sigma_e \geq \sigma_s$, here σ_s is the yield stress and $\sigma_e = (3/2s_{ij}s_{ij})^{1/2}$ is the von Mises effective stress. In order to calculate stress and strain distributions of the welded plate. The results of the thermal analysis step (transient temperature distribution) serve as loading to the corresponding mechanical analysis step. The introduced temperature dependent material mechanical properties Young's Modulus, Poisson's Ration, density and thermal expansion coefficient Table [1] are used. In the mechanical simulation, the elastic behavior is modeled using the isotropic Hooke's rule with temperature-dependent Young's modulus.

3. Results and discussions

3.1 Validation of Transient Temperature Predictions

In order to validate the predicted numerical results a comparison with other experimental results obtained by [15] for same type of aluminum (i.e. 2024 Al) with welding parameters as shown in table [2]and final specimen dimension of $60 \times 50 \times 3\ mm$, these parameters were used as inputs to the ANSYS software.

The numerical thermal analysis is associated with solving the transient three dimensional heat balance equation (Eq. 1) with its associated boundary conditions (Eqs. 6&7) under the effect of moving heat source. An algorithm was created using the ANSYS APDL Macro language to simulate moving heat source. Figures (7 a,b,c,d,e & f) shows contours of temperature variation through FSW process. As the tool moves along the welding line the effect of preheating ahead of the tool is shown throughout the figures. The maximum temperature reach a value of 766 K at the end of welding process prior to cooling in the stirring zone and this value was in good agreement with that predicted experimentally (723 K) with a percent error of 6% by [15].

Figure (8) shows the temperature time history of a point in the HAZ zone, this figure approve the good agreement between that of current study with that of experimental study published by [15]. Peak temperature

resulting from transient thermal analysis is more than experimental results because of the lake of accuracy in modeling of heat transfer during FSW process.
Figure-9 shows the temperature distribution through plate thickness at a time of 50.2 sec, the peak temperature obtained is 766K.
Temperature distributions for four tool positions are shown in figure 10. It can be seen that the peak temperature is increasing with time. This is because of energy trapping in the workpiece.
3.2 Validation of Transient Thermal Residual Stresses
It was assumed that in the thermo-mechanical simulation of FSW process, both thermal process and stress evolution process are sequentially coupled. Where results of the thermal field will be the cause of the driving force that resulting in thermal stresses while thermal solution will not depend on the stress solution. In this case the temperature distribution, which varies in time and space, is loaded into the stress analysis as a predefined field. Temperature fields affect mechanical fields through thermal expansion and temperature dependent material properties. Thermal expansion or contraction due to transient application of temperature gradients is usually the dominant concern in thermal stress analysis.
Figure (11 a,b,c and d) shows the longitudinal residual stress distribution during FSW process and after ending of welding process (cooling). Figures (12 a,b,c and d) and (13 a,b,c and d) show both transverse and Von-Mises stresses. These three stresses show stress evolution that corresponds to temperature distribution shown in figure (11). The figures indicate that localized high temperature underneath tool causes more expansion than the surrounding area. Mutual effect between this area and its surrounding area combined with the effect of clamps will result in variable compression stress along the plate with compression near tool location.
For residual stresses to be determined, clamps were relived gradually for 3 sec during which transient analysis was performed. Longitudinal and transverse residual stresses from ANSYS are shown in figures (14) and (15). The magnitude of the highest longitudinal stress (72 MPa) is around the yield strength of the material at room temperature. Due to high clamping the longitudinal stress reach a value of 319 MPa at the edges. The transverse stress is lower than the longitudinal and therefore takes insignificant importance than longitudinal stresses.

4. Summary and conclusion

A mechanical model was sequentially coupled to a thermal model of the friction stir welding process in order to predicate both temperature distribution and the residual thermal stresses that develop during the welding process. The temperature increases with time on the top surface and decreases with distance perpendicular direction of the tool on the top surface. Longitudinal stress values were found to be the highest compressive stress components. Clamping constraints and locations may have significant localized effects on the stress components in the unaffected parent metal beyond the heat-affected zone.

References

1-H.Schmidt, J. Hattel, J. Wert "An analytical model for the heat generation in friction stir welding" Model. Simul. Mater. Sci. Eng. 12 (2004) 143-157.
2-Y.J. Chao, X. Qi, W. Tang " Heat transfer in friction stir welding : experimental and numerical studies" ASME J. Manuf. Sci. Eng. 125 (2003) 138-145.
3-M. James, M.W. Mahoney, and D. Waldron, 1st Int. Symp. Friction Stir Welding, Thousand Oaks, California, USA, June 14-16 (1999).
4-X.-L. Wang, Z. Feng, S.A. David, S. Spooner and C.R. Hubbard, 6th Int. Conf. Residual Stresses, Oxford, UK, July 10-12 (2000).
5-C.D. Dalle, E. Lima, J. Wegener, A. Pyzalla and T. Buslaps, 3rd Int. Symp on Friction Stir Welding, Kobe Japan, Sept 27-28 (2001).
6-M.A. Sutton, A.P. Reynolds, D.Q. Wang, C.R. Hubbard, A study of residual stresses and microstructure in 2024-T3 aluminum friction stir butt welds, Journal of Engineering Materials and Technology ASME 124 (4) (2002) 215–221.
7-Rui M. Leal and Altino Loureiro, Microstructure and Mechanical Properties of Friction Stir Welds in Aluminum Alloys 2024-T3, 5083-O and 6063-T6, Materials Science Forum, Vols. 514-516 (2006), pp 697-701.
8-P.J. Webster, L.D. Oosterkamp, P.A. Brown, Synchrotron X-ray residual strain scanning of a friction stir weld J. Strain Anal. 36 (1) (2000), pp 61-70.
9-Chao YJ, Qi X, Tang W., Heat transfer in friction stir welding experimental and numerical studies, J. Manuf. Sci. Eng. 125: 138-145.
10-Muhsin Jaber Jweeg, Moneer Hameed Tolephih and Muhammed Abdul-Sattar, Theoretical and Experimental Investigation of Transient Temperature Distribution in Friction Stir Welding of AA 7020-T53, Journal of Engineering, Volume 18, Number 6, June 2012.
11-Soundararajan V, Zekovic S, Kovacevic R (2005) Thermo mechanical model with adaptive boundary

conditions for friction stir welding of Al 6061. Int J Mach Tools Manuf 45:1577–1587
12-P. Prasanna & B. Subba Rao & G. Krishna Mohana Rao, Finite element modeling for maximum temperature in friction stir welding and its validation, Int J Adv Manuf Technol (2010) 51:925–933
13-Zhao Na, Yang Yan-qing, Han Ming, LUO Xian, Feng Guang-hai, Zhang Rong-jun, Finite element analysis of pressure on 2024 aluminum alloy created during restricting expansion-deformation heat-treatment, Trans. Nonferrous Met. Soc. China 22(2012) 2226−2232
14-X.K. Zhu, Y.J. Chao, Numerical simulation of transient temperature and residual stresses in friction stir welding of 304L stainless steel, Journal of Materials Processing Technology 146 (2004) 263–272
15-Saad Ahmed Khodir and Shibayanagi Toshiya, Microstructure and Mechanical Properties of Friction Stir Welded Similar and Dissimilar Joints of Al and Mg alloys, Transactions of JWRI, Vol.36 (2007), No.1

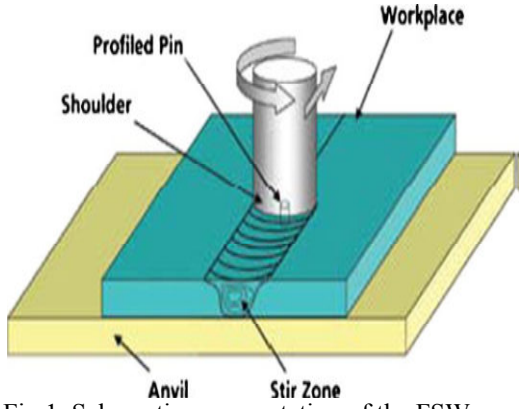

Fig.1. Schematic representation of the FSW process

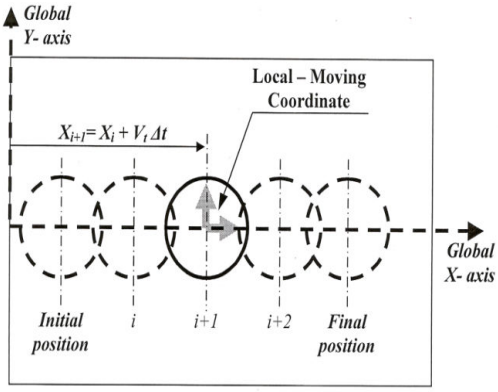

Fig.2. Local Coordinates and Laser Beams Related to the Coordinates

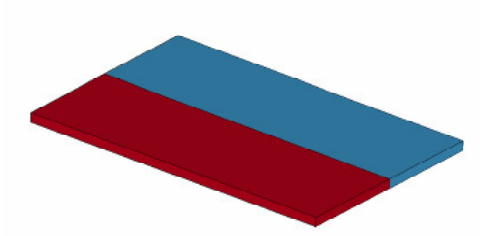

Fig. 3. Geometric Model of Two Plates to be Welded

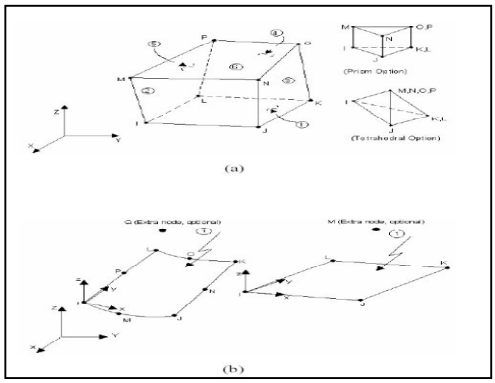

Fig.4. Geometries of: (a) The Three-Dimensional Thermal Solid Element, SOLID70; and (b) The Thermal Surface Effect Element, SURF152.

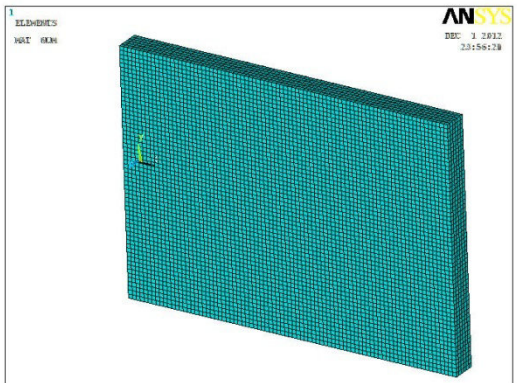

Fig.5. Three-Dimensional Finite Element Model

Table 1 Thermal and mechanical properties of 2024 aluminum alloy

Temperature (^{0}C)	Thermal Conductivity (w m^{-1}K^{-1})	Specific Heat (J Kg^{-1} K^{-1})	Elastic Modulus (GPa)	Poison's Ratio	Yield Strength (MPa)	Density (Kg m^{-3})	Thermal Expansion/ 10^{-6}
20	164	881	72.4	0.33	473	2780	14
100	182	927	66.5	0.33	416.5	2780	23.018
200	194	1047	63.5	0.33	293.5	2780	24.509
300	202	1130	60.4	0.33	239.8	2780	25.119
400	210	1210	56.1	0.33	150	2780	25.594
500	220	1300	50	0.33	100	2780	26.637

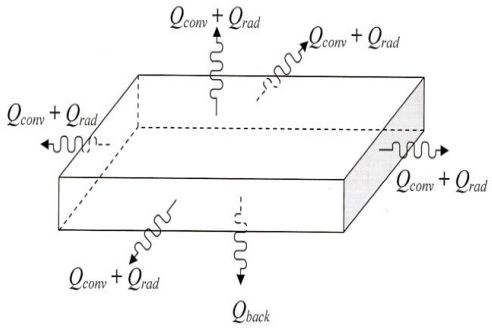

Table [2] Welding Conditions After Reference [15]

Joint type	Rotation speed (min^{-1})	Welding speed (mm/min)	Fixed location of base metals		Welding tool		
			Advancing side	Retreating side	Shoulder diameter	Probe diameter	Tilt angle
Similar 2024 Al alloy joints	400	50	2024 Al alloy	2024 Al alloy	12mm	4 mm	3 degrees

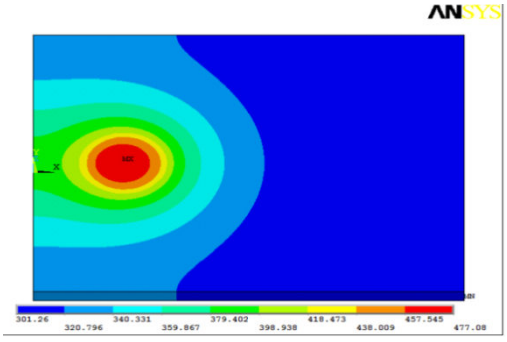

a-

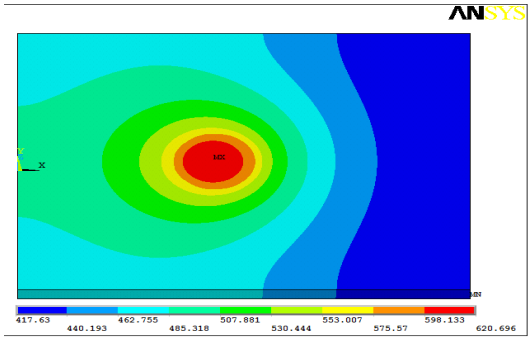

b-

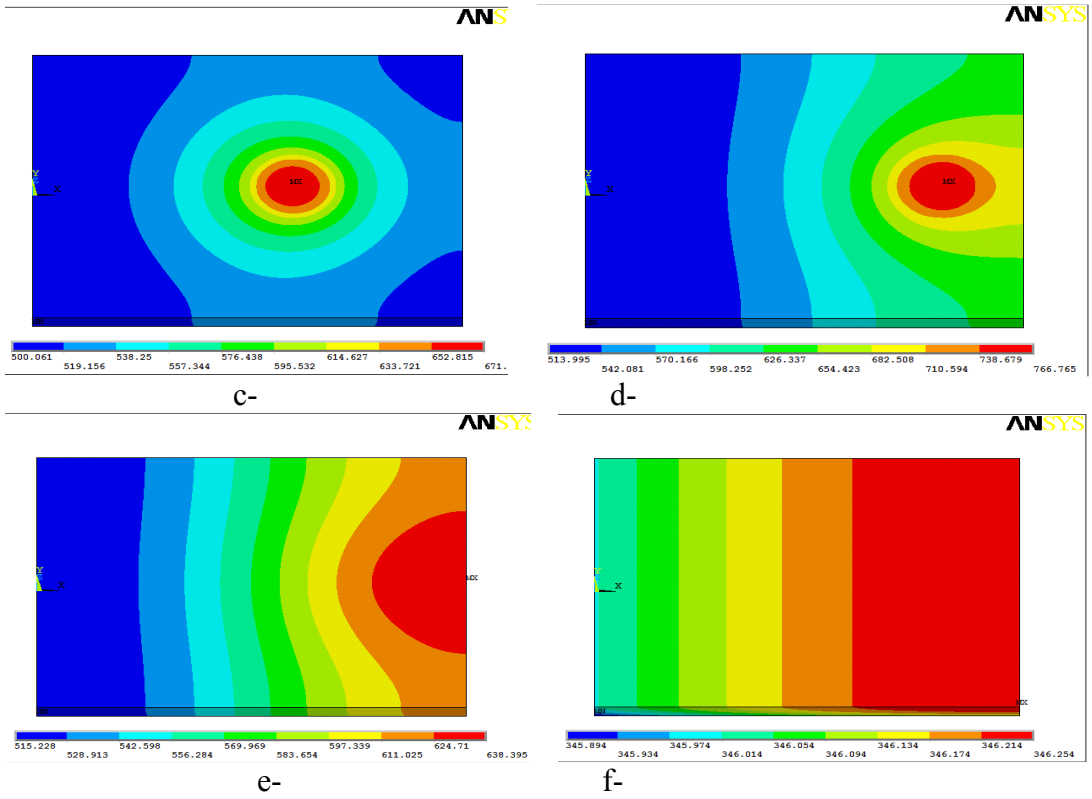

Fig.7.Temperature distributions at:(a)2.2 sec;(b)18.4 sec;(c)30.4 sec;(d)50.2 sec;(e)52.2 sec and(f)125 sec.

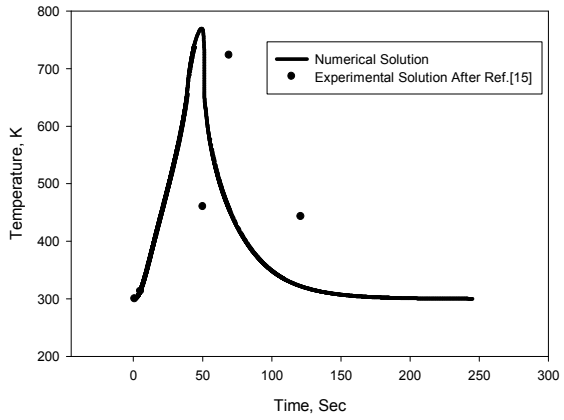

Fig. 8 Temperature time history of a point in the HAZ zone

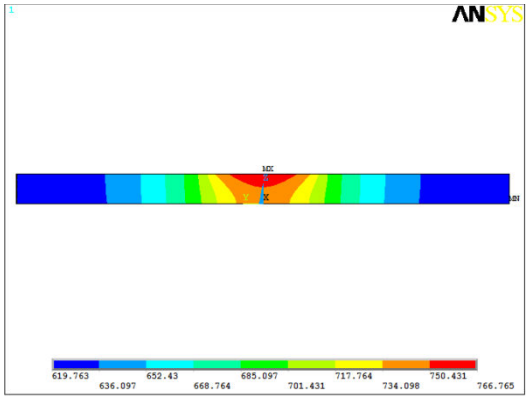

Fig. 9 Calculated isotherms in FSW of Al 2024 at t = 50.2 Sec.

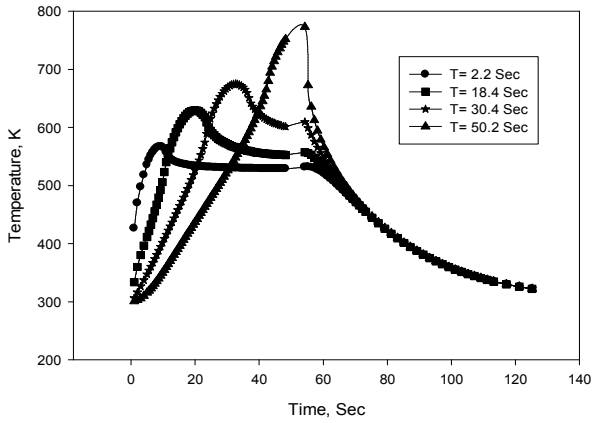

Fig.10 Temperature distributions for four tool positions.

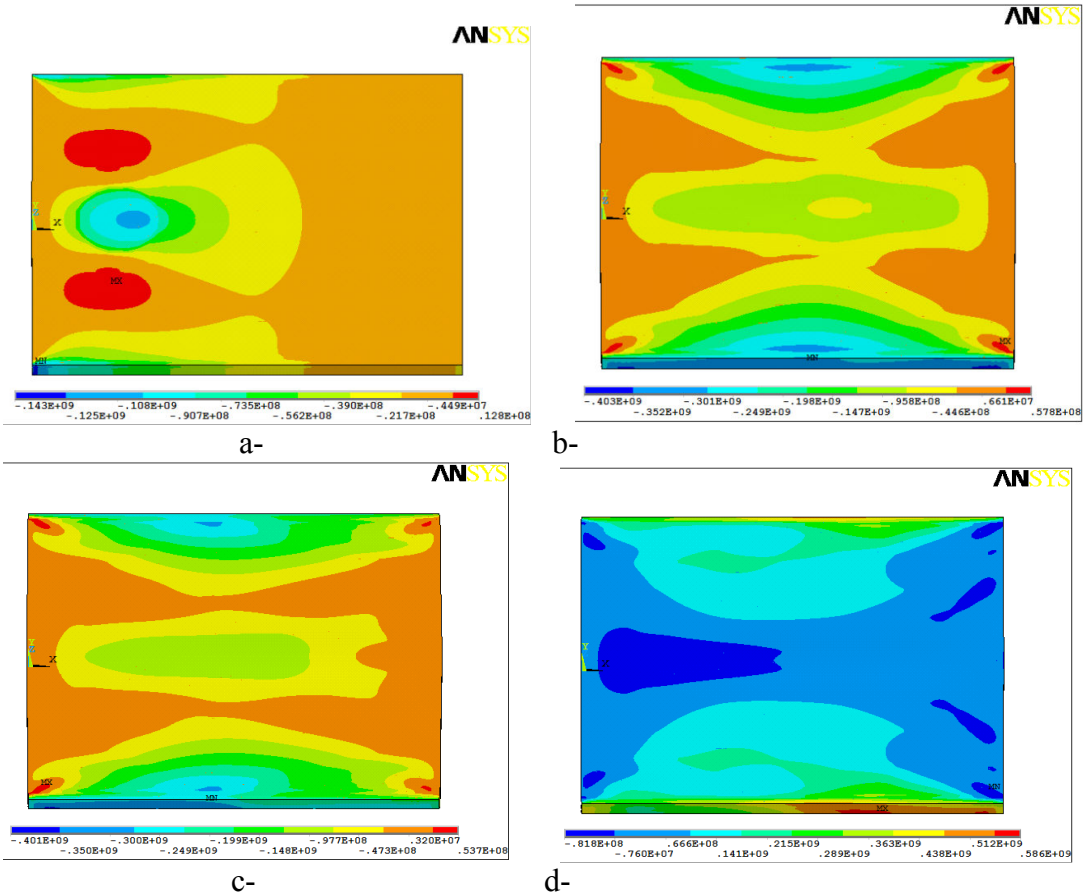

a- b-

c- d-

Fig. (11) Stresses Distribution in x Direction at Time, a) 2.2 Sec (Beginning of Dwell), b) 30.4 Sec (Tool is Moving), c) 50.2 Sec (Tool is Moving) and d) 125 Sec (Cooling of Workpiece)

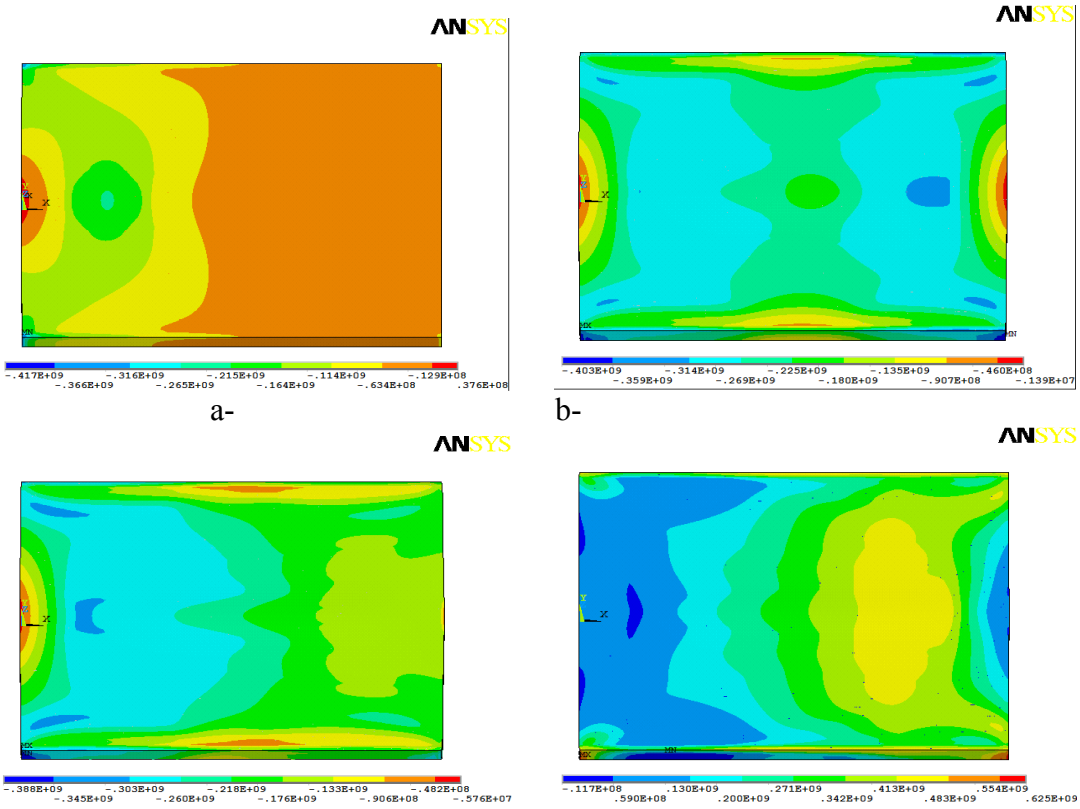

Fig. (12) Stresses Distribution in y Direction at Time, a) 2.2 Sec(Beginning of Dwell), b) 30.4 Sec (Tool is Moving), c) 50.2 Sec (Tool is Moving) and d) 125 Sec (Cooling of Workpiece)

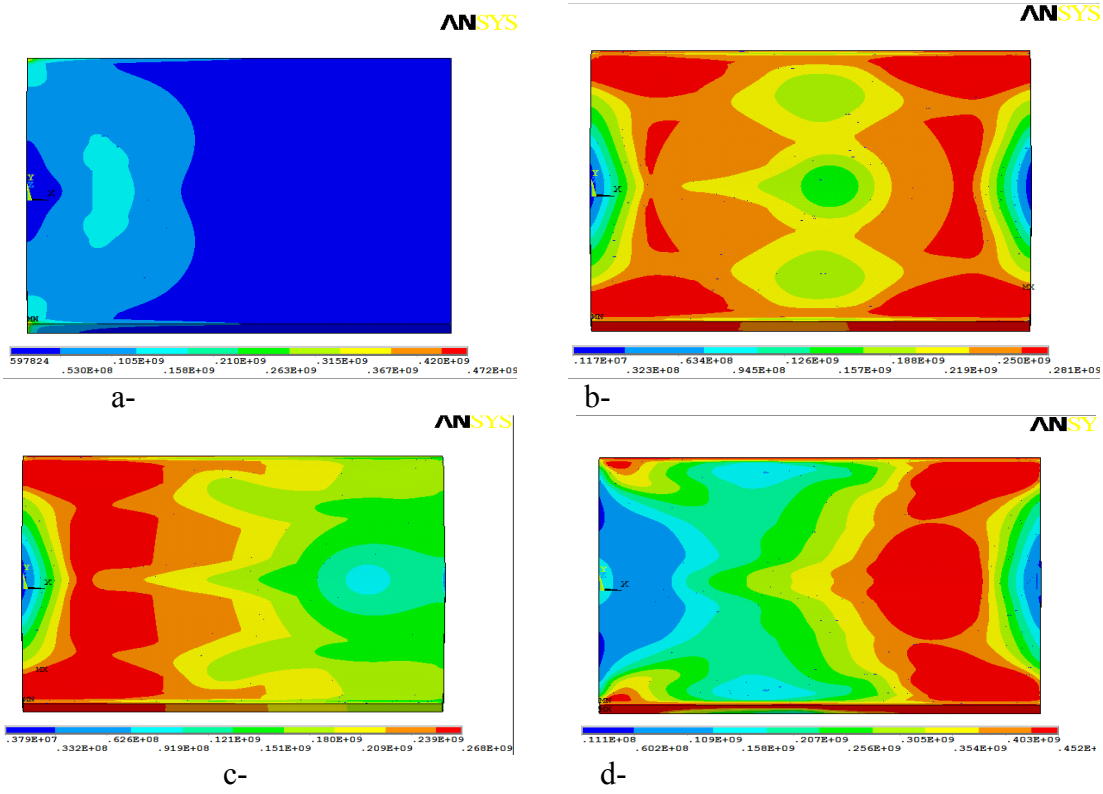

Fig. (13) Von-Mises Stress Distribution at Time, a) 2.2 Sec(Beginning of Dwell), b) 30.4 Sec (Tool is Moving), c) 50.2 Sec (Tool is Moving) and d) 125 Sec (Cooling of Workpiece)

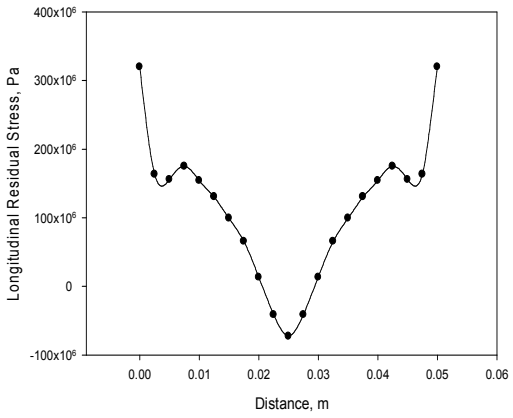

Fig. 14 Longitudinal stress profiles for Al-2024 welds

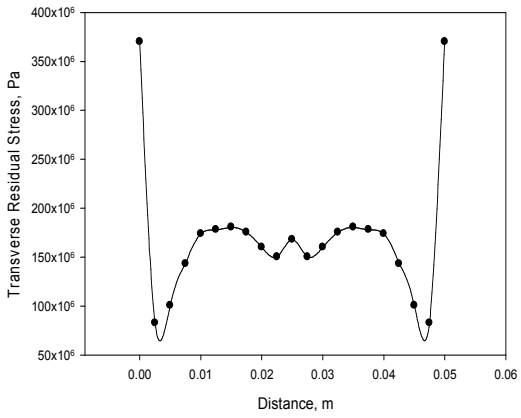

Fig. 15 Transverse stress profiles for Al-2024 welds